

The recent star formation history of the Hipparcos solar neighbourhood

X. Hernandez¹, David Valls-Gabaud² and Gerard Gilmore³

¹ *Osservatorio Astrofisico di Arcetri, Largo E. Fermi 5, 50125 Firenze, Italy*

² *Laboratoire d'Astrophysique, UMR CNRS 5572, Observatoire Midi-Pyrénées, 14 Avenue E. Belin, 31400 Toulouse, France*

³ *Institute of Astronomy, Cambridge University, Madingley Road, Cambridge CB3 0HA, UK*

26 August 2021

ABSTRACT

We use data from the Hipparcos catalogue to construct colour-magnitude diagrams for the solar neighbourhood, which are then treated using advanced Bayesian analysis techniques to derive the star formation history, $SFR(t)$, of this region over the last 3 Gyr. The method we use allows the recovery of the underlying $SFR(t)$ without the need of assuming any *a priori* structure or condition on $SFR(t)$, and hence yields a highly objective result. The remarkable accuracy of the data permits the reconstruction of the local $SFR(t)$ with an unprecedented time resolution of ≈ 50 Myr. A $SFR(t)$ having an oscillatory component of period ≈ 0.5 Gyr is found, superimposed on a small level of constant star formation activity. Problems arising from the non-uniform selection function of the Hipparcos satellite are discussed and treated. Detailed statistical tests are then performed on the results, which confirm the inferred $SFR(t)$ to be compatible with the observed distribution of stars.

Key words: methods: statistical – stars: formation – Solar Neighborhood

1 INTRODUCTION

The problem of deducing the star formation rate history, $SFR(t)$, of the Milky Way has been generally attempted in terms of indirect inferences mostly through chemical evolution models. The validity of these methods relies on the soundness of the assignation of a “chemical age” to each of the studied stars. Generally a metallicity indicator is chosen, and used to measure the metal content of a number of stars which are then binned into age groups through the use of an age-metallicity relation derived from a chemical evolution model. For example, Rocha-Pinto & Maciel (1997) take a variety of age-metallicity relations (AMRs) from the literature and use a closed box chemical evolution model to translate AMRs into $SFR(t)$ s, allowing for an intrinsic Gaussian spread in the AMR assumed to be constant in time.

The advantages of these methods are that large samples of stars both in the solar neighbourhood and further away within the disk of the galaxy can be studied. An inferred $SFR(t)$ can be constructed over an ample time range and spatial extent within the Galaxy which is consistent with the metallicities of the sample studied, and the chemical evolution model proposed. However, the validity of the AMR assumption can not be checked independently of the proposed

chemical evolution model, and is necessarily dependent on what is chosen for the mixing physics of the ISM, the possible infall of primordial non enriched gas, and the still largely unknown galactic formation scenario in general. This last problem also affects attempts at inferring the $SFR(t)$ from stellar kinematics (e.g. Gomez et al. 1990, Marsakov et al., 1990).

With the recent availability of the Hipparcos satellite catalogue (ESA 1997) we are now in a position to attempt recovery of the local $SFR(t)$ directly, without the need of any model dependent assumptions. Previous direct approaches have been undertaken through the binning of observed stars into age groups according to the degree of chromospheric activity as measured through selected emission line features, with conflicting results depending on the assumed age-activity relation (e.g. Barry, 1988, and Soderblom et al., 1991). Using this technique, Rocha-Pinto et al. (1999) have derived a star formation history from the chromospheric activity-age distribution of a larger sample comprising 552 stars, founding evidence for intermittency in the $SFR(t)$ over 14 Gyr. The Hipparcos catalogue offers high quality photometric data for a large number of stars in the solar neighbourhood, which can be used to construct a colour-magnitude diagram (CMD) for this region. Once a CMD is available, it is in principle possible to recover the $SFR(t)$

which gave rise to the observed distribution of stars, assuming only a stellar evolutionary model in terms of a set of stellar tracks. In practice the most common approach to inverting CMDs has been to propose a certain parameterization for the $SFR(t)$, which is used to construct synthetic CMDs, which are statistically compared to the observed ones to select the values of the parameters which result in a best match CMD. Examples of the above are Chiosi et al. (1989), Aparicio et al. (1990) and Mould et al. (1997) using Magellanic and local star clusters, and Mighell & Butcher (1992), Smecker-Hane et al. (1994), Tolstoy & Saha (1996), Aparicio & Gallart (1995) and Mighell (1997) using local dSph's.

We have extended these methods in Hernandez et al. (1999) (henceforth paper I) by combining a rigorous maximum likelihood statistical approach, analogous to what was introduced by Tolstoy & Saha (1996), with a variational calculus treatment. This allows a totally non-parametric solution of the problem, where no *a priori* assumptions are introduced. This method was applied by Hernandez et al. (2000) (paper II) to a set of HST CMDs of local dSph galaxies to infer the $SFR(t)$ of these interesting systems. The result differs from what can be obtained from a chemical evolution model in that a direct answer is available, with a time resolution which depends only on the accuracy of the observations.

Limitations on the applicability of our method to the Hipparcos data appear in connection to the selection function of the catalogue. The need to work only with complete volume-limited samples limits the age range over which we can recover the $SFR(t)$ to 0–3 Gyr, with a resolution of ~ 0.05 Gyr. This makes it impossible to compare our results with those of chemical evolution models which typically sample ages of 0–14 Gyr, with resolutions of 0.5–1.5 Gyr.

In Section 2 we give a summarized review of the method introduced in paper I, the sample selection and results are discussed in section 3. Section 4 presents a careful statistical testing of our results, and Section 5 our conclusions.

2 THE METHOD

In this section we give a summary description of our HR diagram inversion method, which was described extensively in our paper I. In contrast with other statistical methods, we do not need to construct synthetic colour magnitude diagrams for each of the possible star formation histories being considered. Rather we use a direct approach which solves for the best $SFR(t)$ compatible with the stellar evolutionary models assumed and the observations used.

The evolutionary model consists of an isochrone library, and an IMF. Our results are largely insensitive to the details of the latter, for which we use:

$$\rho(m) \propto \begin{cases} m^{-1.3} & 0.08M_{\odot} < m \leq 0.5M_{\odot} \\ m^{-2.2} & 0.5M_{\odot} < m \leq 1.0M_{\odot} \\ m^{-2.7} & 1.0M_{\odot} < m \end{cases} \quad (1)$$

The above fit was derived by Kroupa et al. (1993) for a large sample towards both galactic poles and all the solar neighbourhood, and therefore applies to the Hipparcos data.

As we shall be treating here only data from the so-

lar neighbourhood derived by the Hipparcos satellite, we shall assume for the observed stars a fixed metallicity of $[Fe/H] = 0$. This assumption is valid as we will only be treating stars within a short distance from the Sun, having a small spread in ages. Once the metallicity is fixed we use the latest Padova isochrones (Fagotto et al., 1994, Girardi et al., 1996) together with a detailed constant phase interpolation scheme using only stars at constant evolutionary phase, to construct an isochrone library having a chosen temporal resolution.

To transform the isochrones from the theoretical HR diagram to the observed colour-magnitude diagrams, we used the transformations provided by the calibrations of Lejeune et al. (1997) which are appropriate for the solar metallicities considered here. Using the updated calibrations given by Bessell et al. (1998) does not change the transformations significantly in the regime used here, unlike the case for giant and AGB stars (see Weiss & Salaris, 1999).

In this case we implement the method with a formal resolution of 15 Myr, compatible with the high resolution of the Hipparcos observations. It is one of the advantages of the method that this resolution can be increased arbitrarily (up to the stellar model resolution) with computation times scaling only linearly with it.

Our only other inputs are the positions of, say, n observed stars in the HR diagram, each having a colour and luminosity, c_i and l_i . Starting from a full likelihood model, we first construct the probability that the n observed stars resulted from a certain $SFR(t)$. This will be given by:

$$\mathcal{L} = \prod_{i=1}^n \left(\int_{t_0}^{t_1} SFR(t) G_i(t) dt \right), \quad (2)$$

where

$$G_i(t) = \int_{m_0}^{m_1} \frac{\rho(m; t)}{2\pi\sigma(l_i)\sigma(c_i)} \times \exp\left(\frac{-D(l_i; t, m)^2}{2\sigma^2(l_i)}\right) \exp\left(\frac{-D(c_i; t, m)^2}{2\sigma^2(c_i)}\right) dm$$

In the above expression $\rho(m; t)$ is the density of points along the isochrone of age t , around the star of mass m , and is determined by the assumed IMF together with the duration of the differential phase around the star of mass m . The ages t_0 and t_1 are a minimum and a maximum age needed to be considered, as m_0 and m_1 are a minimum and a maximum mass considered along each isochrone, e.g. 0.6 and 20 M_{\odot} . $\sigma(l_i)$ and $\sigma(c_i)$ are the amplitudes of the observational errors in the luminosity and colour of the i th star. These values are supplied by the particular observational sample one is analysing. Note that for the sample we have selected (Section 3), there is no correlation between these errors. Finally, $D(l_i; t, m)$ and $D(c_i; t, m)$ are the differences in luminosity and colour, respectively, between the i th observed star and a general star of age and mass (m, t) . We shall refer to $G_i(t)$ as the likelihood matrix, since each element represents the probability that a given star, i , was actually formed at time t with any mass.

A similar version was introduced in paper I, but restricted to the case of observational errors only in one variable, which was adequate to the problem of studying the

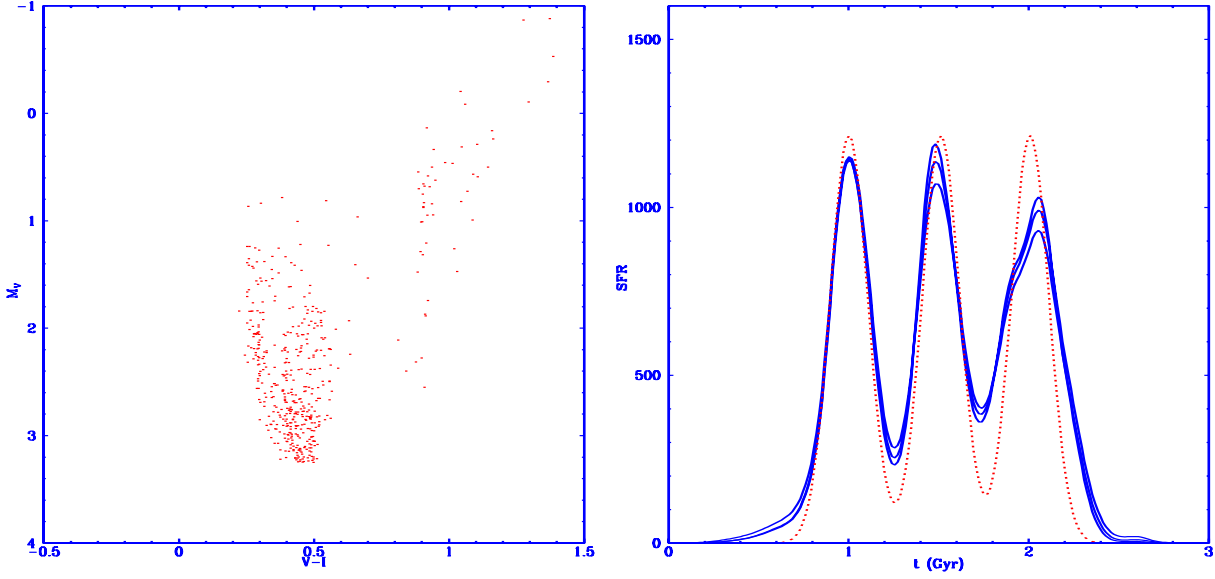


Figure 1.

Left: Simulated colour-magnitude diagram resulting from the first test $SFR(t)$. **Right:** First test $SFR(t)$, dashed line. The solid curves are the last 3 iterations of the method, showing an accurate reconstruction of the input $SFR(t)$.

$SFR(t)$ of local dSph galaxies treated in paper II. Equation (2) is essentially the extension from the case of a discretised $SFR(t)$ used by Tolstoy & Saha (1996), to the case of a continuous function in the construction of the likelihood. The challenge now is to find the optimum $SFR(t)$ without evaluating equation (2) i.e. without introducing a fixed set of test $SFR(t)$ cases from which one is selected.

The condition that $\mathcal{L}(SFR)$ has an extremal can be written as

$$\delta\mathcal{L}(SFR) = 0,$$

and a variational calculus treatment of the problem applied. Firstly, we develop the product over i using the chain rule for the variational derivative, and divide the resulting sum by \mathcal{L} to obtain:

$$\sum_{i=1}^n \left(\frac{\delta \int_{t_0}^{t_1} SFR(t) G_i(t) dt}{\int_{t_0}^{t_1} SFR(t) G_i(t) dt} \right) = 0 \quad (3)$$

Introducing the new variable $Y(t)$ defined as:

$$Y(t) = \int \sqrt{SFR(t)} dt \implies SFR(t) = \left(\frac{dY(t)}{dt} \right)^2$$

and introducing the above expression into equation (3) we can develop the Euler equation to yield

$$\frac{d^2 Y(t)}{dt^2} \sum_{i=1}^n \left(\frac{G_i(t)}{I(i)} \right) = - \frac{dY(t)}{dt} \sum_{i=1}^n \left(\frac{dG_i/dt}{I(i)} \right) \quad (4)$$

where

$$I(i) = \int_{t_0}^{t_1} SFR(t) G_i(t) dt$$

This in effect has transformed the problem from one of searching for a function which maximizes a product of integrals (equation 2) to one of solving an integro-differential equation (equation 4). We solve this equation iteratively, with the boundary condition $SFR(t_1) = 0$.

Details of the numerical procedure required to ensure convergence to the maximum likelihood $SFR(t)$ can be found in our paper I, where a more complete development of the method is also found. In paper I the method was tested extensively using synthetic HR diagrams, obtaining very satisfactory results. Equation (4) will be satisfied by any stationary point in the likelihood, not just the global maximum, it is therefore important to check that the numerical algorithm implemented converges to the true $SFR(t)$. This was shown in our paper I, using synthetic HR diagrams extensively, and testing the robustness of the method to changes in the initialization condition of the algorithm. An independent test of the validity of the results was also implemented, and is described in section 4.

The main advantages of our method over other maximum likelihood schemes are (1) the totally non parametric approach the variational calculus treatment allows, and (2) the efficient computational procedure, where no time consuming repeated comparisons between synthetic and observational CMD are necessary, as the optimal $SFR(t)$ is solved for directly.

2.1 Two tests

We now present two examples of the method's performance, in cases similar to the Hipparcos samples CMDs. The left panel of Figure (1) shows a synthetic CMD produced from the first input $SFR(t)$, resulting in a number of stars similar

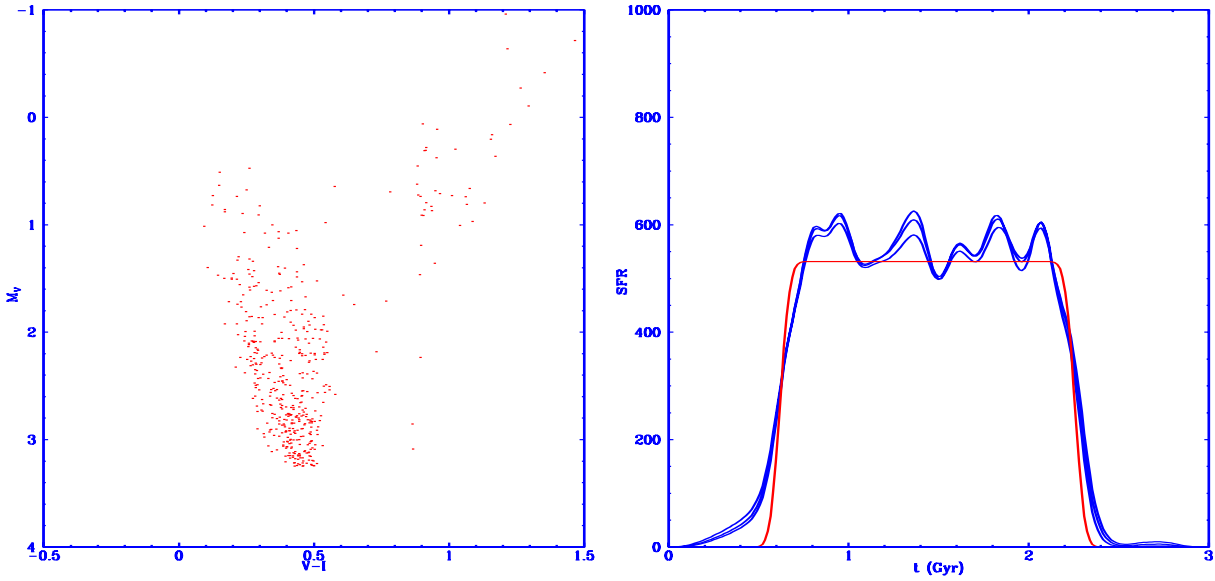


Figure 2.

Left: Simulated CMD resulting from the second test $SFR(t)$. **Right:** Second test $SFR(t)$, dashed line. The solid curves are the last 3 iterations of the method, showing an accurate reconstruction of the input $SFR(t)$.

to what the Hipparcos samples yield for small errors in $V - I$ (< 0.12 mag) and M_V (< 0.02 mag). The positions of the simulated stars are then used to construct the likelihood matrix, which is used to recover the inferred $SFR(t)$, through an iterative numerical procedure (see paper I). The right panel of Figure (1) shows the last 3 iterations of the method (solid curves) and the input $SFR(t)$, a three burst $SFR(t)$ (dotted curve). It can be seen that the main features of the input $SFR(t)$ are accurately recovered. The age, duration and shape of the input $SFR(t)$ are clearly well represented by the final inferred $SFR(t)$. As the difference between successive isochrones diminishes with age, since the errors remain constant, the accuracy of the recovery procedure diminishes with the age of the stellar populations being treated. This is seen in that the first burst is very accurately recovered, whilst the last one appears somewhat spread out.

The last example is shown in Figure (2), which is analogous to Figure (1). Here a $SFR(t)$ which is constant over a large period is treated. The HR diagram of this case appears by sight almost identical to that of the previous case, however, given the extremely small errors assumed (typical of the Hipparcos data) the method is capable of distinguish and accurately recover the input $SFR(t)$ of these two cases. The small number of stars (~ 450) result in a degree of shot noise, which has to be artificially suppressed using a smoothing procedure, the result of which is seen in the residual short period oscillations of the inferred $SFR(t)$. This smoothing procedure reduces the effective resolution of the method to 50 Myr. Note that as in the previous example, the inversion method successfully recovers the main features of the input $SFR(t)$. In these two tests only stars bluewards of $V - I = 0.7$ were considered in the inversion procedure (see below).

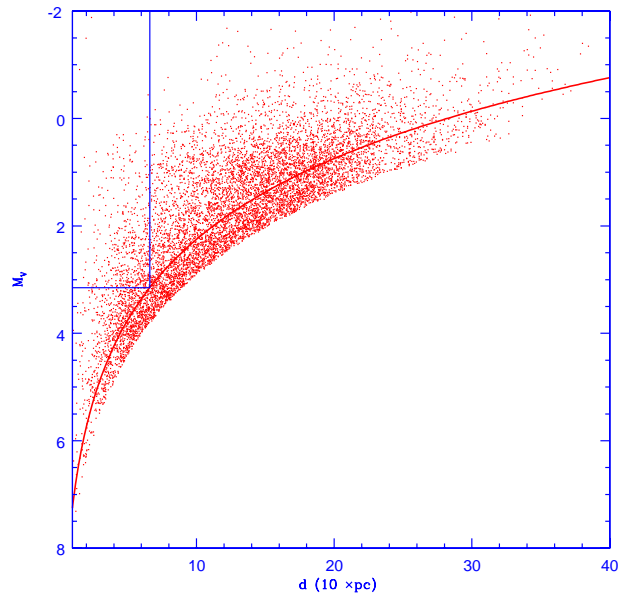


Figure 3. Stars in the Hipparcos catalogue having distance errors $< 20\%$. The sharp lower envelope shows the completeness limit of $m < 7.9$. The straight lines show one volume limited sample, at $M_V < 3.15$. The curve shows the completeness limit of $m < 7.25$, which corresponds to errors similar to what was used in the simulations of Figures (1) and (2).

3 SAMPLE SELECTION AND RESULTS

In order to apply the method described in the preceding section to the Hipparcos data, we would like to construct a volume-limited sample, where no biases appear between stars of different ages. Further, such a sample should contain a sufficient number of stars coming from all age groups being considered i.e. it must go down in magnitude to the turnoff point corresponding to the oldest age being considered. Although the Hipparcos satellite produced a catalogue having very well understood errors and highly accurate magnitude and colour determinations for a large number of stars, the sample has to be reduced through several cuts before it complies with the restrictions required by our method.

The Hipparcos catalogue provides an almost complete sample of stars in the solar neighbourhood. The limiting magnitude depends both on spectral type and galactic latitude (ESA SP-1200, Volume 1, page 131). For the types earlier than G5 which we consider here, the limiting V magnitude is given by $V_{\text{lim}} = 7.9 + 1.1 \sin |b|$. To avoid unnecessary complications, we consider cuts of the type $V = \text{const.}$ at all latitudes with $V < 7.9$.

Figure (3) shows a graph of M_V vs. distance for all stars in the Hipparcos catalogue having distance errors smaller than 20%, and an apparent magnitude $m_V < 7.9$. The solid lines show the inclusion criteria for one possible volume limited sample, complete to $M_V < 3.15, m < 7.25$. As it can be seen, the maximum age which can be considered will not be very large, as the number of stars in a volume-limited sample complete to absolute magnitudes greater than 4 rapidly dwindles. After experimenting with synthetic CMDs of known $SFR(t)$ produced using our isochrone grid and constructed to have the same numbers of stars as a function of lower magnitude limit as in Figure (3), and recovering the $SFR(t)$ using our method, we identified 3 Gyr as the maximum age we can accurately treat with the data at hand. This fixes $t_0 = 0, t_1 = 3$ Gyr as the temporal limits in equation (2), were the use of 200 isochrones establishes the formal resolution of the method to be 15 Myr.

Although the absolute magnitude errors correlate tightly with the distance, the colour errors correlate more strongly with the apparent magnitude, and can actually represent the dominant error in inverting the CMDs. The solid curve shows the $m_V < 7.25$ completion limit, which implies errors similar to those used in Figures (1) and (2). It will be with complete volume-limited samples having this apparent magnitude limit that we will be dealing.

As the limit in M_V is moved to dimmer stars, the structure of the $SFR(t)$ at older ages is better recovered by the inversion method, but the number of younger stars diminishes (see Figure 1) and the $SFR(t)$ of the younger period is under represented in the recovered $SFR(t)$. We constructed a variety of somewhat independent Hipparcos CMDs for different absolute magnitude limits in the range $3.0 < M_V < 3.5$, and obtained highly compatible answers.

Also, all our samples include a certain number of contaminating stars having ages greater than the 3 Gyr limit considered by the inversion method, mostly in the RGB region, as their turn off points appear at magnitudes dimmer than the minimum ones considered. To avoid these stars, the inversion method considers only stars bluewards

of $V - I = 0.7$, as was done in the synthetic examples of Figures (1) and (2).

As the fraction of stars produced by the $SFR(t)$ which live into the observed CMD diminishes with age, in inverting a well populated CMD the older regions of the $SFR(t)$ are under estimated by the recovery method. This is compensated by a correction factor given by the assumed IMF, and the mass at the tip of the RGB as a function of time, as discussed in paper I.

Once the IMF, metallicity, positions of the observed stars in the CMD and observational errors in both coordinates (also supplied by the Hipparcos catalogue) are given, they are used to construct the likelihood matrix $G_i(t)$, which is the only input given to the inversion method. The small number of stars present in any volume-limited sample (~ 450) leaves us insensitive to the existence of small features in the $SFR(t)$ producing only a few stars. The limited numbers of stars also reduces the resolution of the method, as a smoothing function has to be applied to suppress instabilities in solving the integro-differential equation of the problem. This final smoothing reduces the effective temporal resolution of the method to 50 Myr, still much higher than that of any indirect chemical evolution inference of $SFR(t)$.

3.1 Kinematic and geometric corrections

Once the apparent and absolute magnitudes of the sample have been chosen, the set of stars to be studied is fully specified. The positions of which in the CMD are compared to the assumed isochrones to construct the likelihood matrix, which is the only input required by the numerical implementation of the method, as described above. The resulting $SFR(t)$ will be representative of the stars which were used in the construction of the likelihood matrix.

To normalize the various inferred $SFRs(t)$ from samples having different M_V limits, and hence complete out to different distances, we apply the following kinematic and geometric corrections.

Let $F(v, h)$ be the fraction of the time a star having vertical velocity at the disk plane v spends between heights $-h$ and $+h$. Then, for a cylindrical sample complete to height h above and below the disk plane,

$$N(t) = \frac{N_o(t)}{\sqrt{2\pi} \sigma(t)} \int_{-\infty}^{\infty} \frac{e^{-v^2/2\sigma(t)^2}}{F(v, h)} dv \quad (5)$$

where $N(t)$ is the number of stars a stellar population of age t contains, $N_o(t)$ the number of stars of age t observed and $\sigma(t)$ the time dependent velocity dispersion of the several populations. As volume-limited samples are generally spherical around the Sun, a further geometric factor is required, giving:

$$N(t) = \frac{3N_o(t)}{2\sqrt{2\pi} \sigma(t) R^3} \int_0^R r h \int_{-\infty}^{\infty} \frac{e^{-v^2/2\sigma(t)^2}}{F(v, h)} dv dr \quad (6)$$

where R is the radius of the observed spherical volume limited sample, r is a radial coordinate and $h^2 = R^2 - r^2$. To estimate $F(v, h)$ one requires the detailed vertical force law of the galactic disk at the solar neighbourhood. The best direct estimate of this function remains that of Kuijken and Gilmore (1989), who show this function to deviate from that of a harmonic potential to a large degree. This detailed

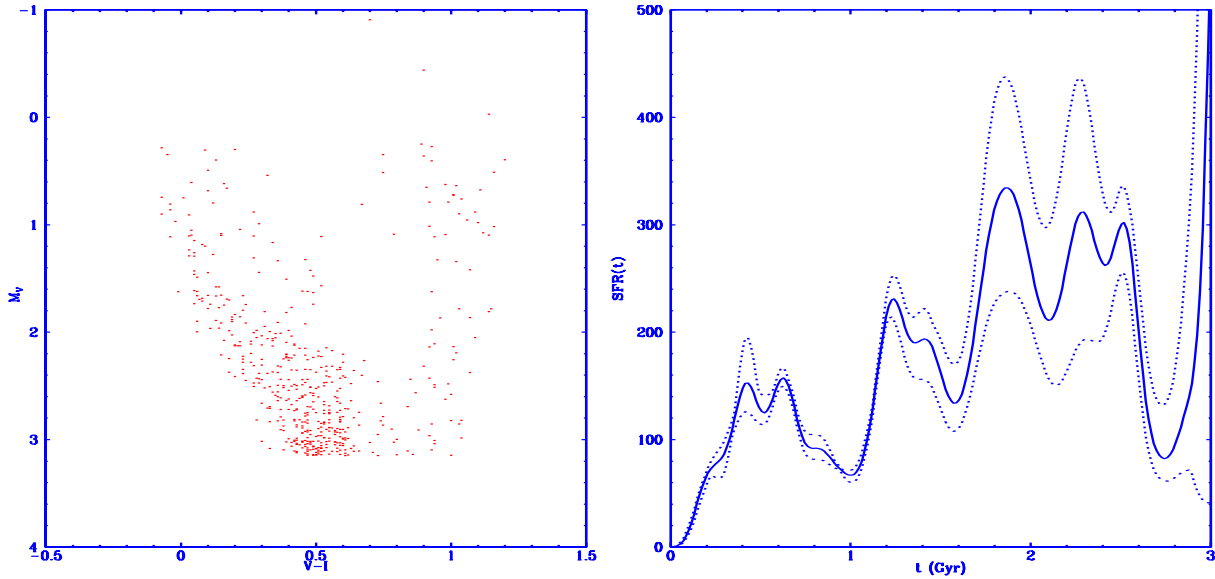


Figure 4.

Left: Colour-magnitude diagram of the volume-limited sample complete to $M_V < 3.15$ from the Hipparcos satellite. **Right:** Inferred $SFR(t)$ resulting from this dataset. Only stars bluewards of $V - I = 0.7$ were considered in the inversion procedure, representative of the last 3 Gyr.

force law we integrate numerically to obtain $F(v, h)$. We use $\sigma(t) = 20$ km/s which is appropriate for the metallicity and age ranges we are studying (Edvardsson et al. 1993, Wyse & Gilmore 1995). Note also that the scatter in metallicity within 80 pc is rather small (Garnett and Koblunicky, 1999) and will not change significantly our results.

In this way, assuming a Gaussian distribution for the vertical velocities of the stars, and a given $\sigma(t)$, an observed $N_o(t)$ can be transformed into a total $N(t)$, which is equal to the total projected disk quantity.

In our case the $SFR(t)$ given by the method takes the place of $N_o(t)$, and equation (6) is used to obtain a final star formation history, which accounts for the kinematic and geometric factors described. This function is then normalized through the total number of stars in the relevant sample, to give the deduced $SFR(t)$ in units of $M_\odot \text{Myr}^{-1} \text{kpc}^{-2}$.

3.2 Results

Figure (4) shows the CMD corresponding to a volume-limited sample complete to $M_V < 3.15$ for stars in the Hipparcos catalogue having errors in parallax of less than 20% and $m_V < 7.25$ (left panel). The right panel of this figure shows the result of applying our inversion method to this CMD, solid curve. The dotted envelope encloses several alternative reconstructions arising from different M_V cuts, and gives an estimate of the errors likely to be present in our result, which can be seen to increase with time. The reconstruction based on the $(M_V, B - V)$ diagram gives essentially the same results.

A certain level of constant star formation activity can be seen, superimposed onto a strong, quasi-periodic compo-

nent having a period close to 0.5 Gyr, as encoded in the positions of the observed stars in the CMD. The sharp feature seen towards $t = 3$ Gyr could be the beginning of a fifth cycle, truncated by the boundary condition $SFR(3) = 0$. We have performed tests with synthetic CMDs having the same numbers of stars and magnitude limits as in Figure (4), and having a variety of $SFR(t)$. The method efficiently discriminates between constant and periodic input $SFR(t)$, and correctly recovers features such as those found in the inferred $SFR(t)$ of Figure (4). We conclude that as far as the Padova isochrones at solar metallicity are representative of the observational properties of the stars in the CMDs, the $SFR(t)$ of the solar neighbourhood over the last 3 Gyr has been that shown in Figure (4). The unprecedented time resolution of our SFR reconstruction makes it difficult to compare with the results derived from chromospheric activity studies (Rocha-Pinto et al. 1999), although qualitatively we do find the same activity at both 0.5 and above 2 Gyr, but not the decrease between 1 and 2 Gyr.

One possible interpretation of a cyclic component in the $SFR(t)$ of the solar neighbourhood can be found in the density wave hypothesis (Lin and Shu, 1964) for the presence of spiral arms in late type galaxies. As the pattern speed and the circular velocity are in general different, a given region of the disk (e.g. the solar neighbourhood), periodically crosses an arm region where the increased local gravitational potential might possibly trigger an episode of star formation. In the simplest version of this scenario, we can take the pattern angular frequency Ω_p equal to twice the circular frequency Ω at the Sun's position (Binney & Tremaine 1987), valid within a flat rotation curve region. The time interval Δt between encounters with an arm at the solar neighbourhood

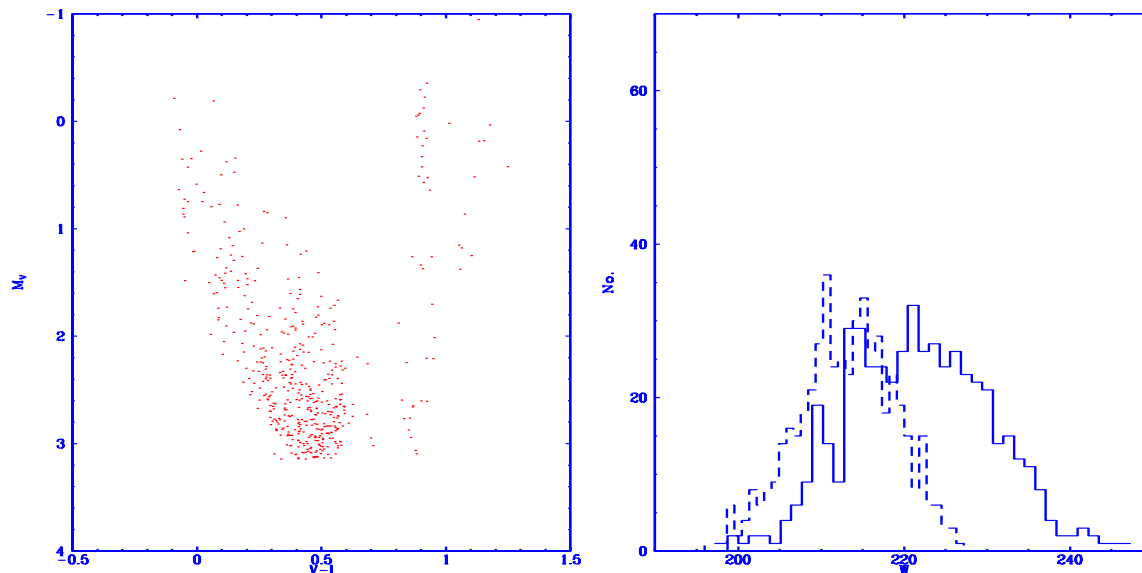


Figure 5.

Left: Simulated CMD from the inferred $SFR(t)$, down to $M_V < 3.15$ containing a similar number of stars to the volume limited sample complete to the same limit. **Right:** Histogram of W statistics for 500 model-model comparisons, solid curve. The dashed histogram gives the W statistics of 500 data-model comparisons, showing the inferred $SFR(t)$ to be compatible with this volume-limited sample.

will be given in general by

$$\Delta t = \frac{2\pi}{m|\Omega - \Omega_p|}$$

that is,

$$\Delta t = \frac{0.22 \text{ Gyr}}{m} \left(\frac{\Omega}{29 \text{ km s}^{-1} \text{ kpc}^{-1}} \right)^{-1} \left| \frac{\Omega_p}{\Omega} - 1 \right|^{-1}$$

where m is the number of arms in the spiral pattern. The classical value of the pattern speed, $\Omega_p = 0.5 \Omega \approx 14.5 \text{ km s}^{-1} \text{ kpc}^{-1}$ would imply that the interaction with a single arm ($m = 1$) would be enough to account for the observed regularity in the recent SFR history. However, more recent determinations tend to point to much larger values (e.g. Mishkurov et al. 1979, Avedisova 1989, Amaral and Lépine 1997) close to $\Omega_p \sim 23 - 24 \text{ km s}^{-1} \text{ kpc}^{-1}$, which would then imply that the regularity present in the reconstructed $SFR(t)$ would be consistent with a scenario where the interaction of the solar neighbourhood with a two-armed spiral pattern would have induced the star formation episodes we detect. These arms are clearly detected in, for instance, the distribution of free electrons in the galactic plane (Taylor and Cordes 1993). This is reminiscent of the explanations put forward to account for the inhomogeneities observed in the velocity distribution function, where well-defined branches associated with moving groups of different ages (Chereul et al. 1999, Skuljan et al. 1999, Asiain et al. 1999) could perhaps be also associated with an interaction with spiral arm(s), although in this case the time scales are much smaller.

Alternatively, if the solar neighbourhood is closer to the corotation radius, the galactic bar could have triggered star

formation in the solar neighbourhood with episodes separated by about 0.5 Gyr if the pattern speed of the bar is larger than about $40 \text{ km s}^{-1} \text{ kpc}^{-1}$ (Dehnen 1999).

Of course, other explanations are possible, for example the cloud formation, collision and stellar feedback models of Vazquez & Scalo (1989) predict a phase of oscillatory $SFR(t)$ behaviour as a result of a self-regulated star formation régime. Close encounters with the Magellanic Clouds have also been suggested to explain the intermittent nature of the SFR on longer time scales (Rocha-Pinto et al. 2000).

We have tested the ability of our method to accurately distinguish oscillatory components in the $SFR(t)$ with tests such as those shown in Figures (1) and (2). The oscillatory component in the case shown in Figure (1) is successfully recovered by the method. In the case shown in Figure(2) however, although the main features are also accurately recovered, a level of small amplitude fluctuations spuriously appears. This last feature is of such a small level, that if a CMD where produced from the method answer of Figure (1) having the same total number of stars, each small fluctuation would produce a number of stars of order 1.

Our answer shown in Figure (4) shows not only a large scale oscillatory component, but superimposed onto this, a certain level of small amplitude fluctuations. Given the total number of stars present in our sample, we can not rule out the possibility (quite possibly in fact the case) that these small fluctuations are numerical, as they are of amplitude similar to the ones discussed appearing in Figure(2), and are actually buried within the error envelope. The main oscillatory component having a period of 0.5 Gyr however, involves a sufficiently large number of stars to be objectively identified.

A larger and independent data set from which to derive $SFR(t)$ would be necessary in order to extend our results to a broader age range, and a more extensive region of the Galactic disk. Increasing the number of stars available for the HR inversion procedure would also allow to recover finer features, and reduce the small numerical fluctuations discussed above.

4 TESTING THE RESULTS

In our Paper I we tested this method using synthetic CMDs produced from known star formation histories, with which we could assess the accuracy of the result of the inversion procedure, as shown in Figures (1) and (2). In working with real data, we require the introduction of an independent method of comparing our final result to the starting CMD, in order to check that the answer our inversion procedure gives is a good answer. From our paper I we know that when the stars being used in the inversion procedure were indeed produced from the isochrones and metallicity used to construct the likelihood matrix, the inversion method gives accurate results. The introduction of an independent comparison between our answer and the data is hence a way of checking the accuracy of the input physics used in the inversion procedure, i.e. the IMF, metallicity and observational parameters.

The most common procedure of comparing a certain $SFR(t)$ with an observed CMD is to use the $SFR(t)$ to generate a synthetic CMD, and compare this to the observations using a statistical test to determine the degree of similarity between the two.

The disadvantage however is that one is not comparing the $SFR(t)$ with the data, but rather a particular realisation of the $SFR(t)$ with the data. The distinction becomes arbitrary when large numbers of stars are found in all regions of the CMD, which is generally not the case. Following a Bayesian approach, we prefer to adopt the W statistic presented by Saha (1998), essentially

$$W = \prod_{i=1}^B \frac{(m_i + s_i)!}{m_i!s_i!}$$

where B is the number of cells into which the CMD is split, and m_i and s_i are the numbers of points two distributions being compared have in each cell. This asks for the probability that two distinct data sets are random realisations of the same underlying distribution. In implementing this test we first produce a large number (500) of random realisations of our inferred $SFR(t)$, and compute the W statistic between pairs in this sample of CMD's. This gives a distribution which is used to determine a range of values of W which are expected to arise in random realisations of the $SFR(t)$ being tested. Next the W statistic is computed between the observed data set, and a new large number of random realisations of $SFR(t)$ (also 500), this gives a new distribution of W which can be objectively compared to the one arising from the model-model comparison to assess whether both data and modeled CMD's are compatible with a unique underlying distribution.

Figure (5) shows a synthetic CMD produced from our

inferred $SFR(t)$ for the solar neighbourhood, down to $M_V = 3.15$. This can be compared to the Hipparcos CMD complete to the same M_V limit of Figure (4). A visual inspection reveals approximately equal numbers of stars in each of the distinct regions of the diagram, a more rigorous statistical comparison is also included. The right panel of Figure (5) shows a histogram of the values of the W statistic for 500 random realisations of our inferred $SFR(t)$ in a model-model comparison. This gives the range of values of the W statistic likely to appear in comparisons of two CMD diagrams arising from the same underlying $SFR(t)$, our inferred $SFR(t)$. The dashed histogram shows the results of 500 synthetic CMDs vs. the observed Hipparcos data set. The compatibility of both sets of W values is clear. In this way the observed stars in the volume limited sample complete to $M_V = 3.15$ and the isochrones, IMF and metallicity used in estimating the inferred $SFR(t)$ shown in Figure (4) are shown to be compatible with each other. Similar tests were also performed changing the limiting M_V in the range 3.0 – 3.5, and comparing against the corresponding Hipparcos sample. This produces alternative CMDs which contain different stars (see Figure 3), which were compared to synthetic CMDs coming always from the same central inferred $SFR(t)$. The results were always equal or better than what is shown in Figure 5, model-model and data-model distributions of W having mean values well within 1σ of each other, where σ refers to either the model-model or the data-model W distributions.

5 CONCLUSION

We have applied the method developed in our paper I to the data of the Hipparcos catalogue. An objective answer for the $SFR(t)$ of the solar neighbourhood over the last 3 Gyr was found, which can be shown to be consistent with the complete volume-limited Hipparcos samples relevant to this age range. A structured $SFR(t)$ is obtained showing a cyclic pattern having a period of about 0.5 Gyr, superimposed on some degree of underlying star formation activity which increases slightly with age. No random bursting behaviour was found at the time resolution of 0.05 Gyr of our method. A first order density wave model for the repeated encounter of galactic arms could explain the observed regularity.

REFERENCES

- Asiani R., Figueras F., Torra J., 1999, A&A, 350, 434
Amaral L.H., Lépine J.R.D., 1997, MNRAS, 286, 885
Aparicio A., Bertelli G., Chiosi C., Garcia-Pelayo J.M., 1990, A&A 240, 262
Aparicio A., Gallart C., 1995, AJ, 110, 2105
Avedisova V.S., 1989, Astrophys. 30, 83
Barry D.C., 1988, ApJ, 334, 436
Bessell, M.S., Castelli, F., Plez, B. 1998, A&A 333, 231
Binney J., Tremaine S., 1987, Galactic Dynamics. Princeton Univ. Press, Princeton
Chereul E., Crézé M., Bienaymé O., 1999, A&A Suppl. 135, 5
Chiosi C., Bertelli G., Meylan G., Ortolani S., 1989, A&A, 219, 167
Dehnen W., 1999, ApJ, 524, L35
Edvardsson B., Andersen. J., Gustafsson. B., Lambert. D.L., Nissen. P., Tomkin. L., 1993, A&A, 275, 101

- ESA, 1997, The Hipparcos catalogue, ESA SP-1200
- Fagotto F., Bressan A., Bertelli G., Chiosi C., 1994, *A&AS*, 104, 365
- Garnett D.R., Kobulnicky H.A., 1999, *ApJ Lett*, in press (astro-ph/9912031)
- Girardi L., Bressan A., Chiosi C., Bertelli G., Nasi E., 1996, *A&AS* 117, 113
- Gomez A.E., Dehaye J., Grenier S., Jaschek C., Arenou F., Jaschek M., 1990, *A&A*, 236, 95
- Hernandez X., Valls-Gabaud D., Gilmore G., 1999, *MNRAS*, 304, 705 (paper I)
- Hernandez X., Gilmore G., Valls-Gabaud D., 2000, *MNRAS*, in press (astro-ph/0001337)
- Kroupa P., Tout C.A., Gilmore G., 1993, *MNRAS*, 262, 545
- Kuijken K., Gilmore G. 1989, *MNRAS*, 239, 571
- Lejeune T., Cuisinier, F. Buser, R. 1997, *A&AS* 125, 229
- Lin C.C., Shu F.H., 1964, *ApJ*, 140, 646
- Marsakov V.A., Shevelev Yu.G., Suchkov A.A., 1990, *Ap&SS*, 172, 51
- Mighell K.J., Butcher H.R., 1992, *A&A*, 255, 26
- Mighell K.J., 1997, *AJ*, 114, 1458
- Mishkurov Y.N., Pavloskaya E.D., Suchkov A.A., 1979, *AZh*, 56, 268
- Mould J.R., Han M., Stetson P.B., 1997, *ApJ*, 483, L41
- Rocha-Pinto H.J., Maciel W.J., 1997, *MNRAS*, 289, 882
- Rocha-Pinto H.J., Scalo J., Maciel W.J., Flynn C., 1999, *ApJ Lett* submitted (astro-ph/9908328)
- Rocha-Pinto H.J., Scalo J., Maciel W.J., Flynn C., 2000, *A&A*, submitted (astro-ph/0001383)
- Saha P., 1998, *AJ*, 115, 1206
- Skuljan J., Hearnshaw J.B., Cottrell P.L., 1999, *MNRAS*, 308, 731
- Soderblom D.R., Duncan D.K., Johnson D.R., 1991, *ApJ* 375, 722
- Smecker-Hane T.A., Stetson P.B., Hesser J.E., Lehnert M.D., 1994, *AJ*, 108, 507
- Taylor J.H., Cordes J.M., 1993, *ApJ*, 411, 674
- Tolstoy E., Saha A., 1996, *ApJ*, 462, 672
- Vazquez E.C., Scalo J.M., 1989, *ApJ*, 343, 644
- Weiss, A., Salaris, M. 1999, *A&A*, 346, 897
- Wyse, R.F.G., Gilmore, G., 1995, *AJ*, 110, 2771